# LOVTRAP: an optogenetic system for photoinduced protein dissociation

Hui Wang[1,9], Marco Vilela[2,9], Andreas Winkler[3,8], Miroslaw Tarnawski[3], Ilme Schlichting[3], Hayretin Yumerefendi[4], Brian Kuhlman[4], Rihe Liu[5,6], Gaudenz Danuser[2] & Klaus M Hahn[1,7]



**LOVTRAP is an optogenetic approach for reversible light-induced protein dissociation using protein A fragments that bind to the LOV domain only in the dark, with tunable kinetics and a >150-fold change in the dissociation constant ($K_d$). By reversibly sequestering proteins at mitochondria, we precisely modulated the proteins' access to the cell edge, demonstrating a naturally occurring 3-mHz cell-edge oscillation driven by interactions of Vav2, Rac1, and PI3K proteins.**

The control of proteins with light has been extended beyond engineering of light-sensitive ion channels to activation of nonchannel proteins through fusion with light-sensitive plant proteins[1]. This has revealed important roles for transient subcellular localization and activation kinetics in signaling[1]. Here we describe LOV2 trap and release of protein (LOVTRAP), an optogenetic approach capable of repeatedly and reversibly controlling protein activity with precise kinetics. This approach uses a small protein, which we named Zdark (Zdk), generated by mRNA display screening of a library derived from the Z subunit of protein A. Zdk binds selectively to the dark state of LOV2, a photosensor domain from *Avena sativa* phototropin 1. We anchored either Zdk or LOV2 away from the site where the protein of interest (POI) acted and fused the POI to the nonanchored member of the pair (**Fig. 1a**). In the dark the POI was sequestered away from its site of action; upon irradiation, Zdk dissociated from LOV2, freeing the POI to move to its site of action. This approach improves upon previously available methods, as it provides diffusion-limited activation kinetics (proteins are released in less than a second), and deactivation rates can be tuned from seconds to minutes using mutations described below. The approach is broadly applicable, as the POI simply needs to be fused to either LOV or Zdk. The method reduces 'leakiness', or dark-state background activity. Anchored LOV2 can be expressed in excess of the POI, so that even if a small equilibrium amount of LOV2 is in the 'lit' (nonbinding) conformation in the dark, there is still sufficient anchored LOV2 to sequester the POI (**Supplementary Note** and **Supplementary Fig. 1**). Finally, proteins are not controlled through light-induced delivery to specific subcellular locations; hence, they can act at multiple sites upon activation.

We generated Zdk using a library based on the Z domain of immunoglobulin-binding staphylococcal protein A[2]. The Z domain is a small, tightly folded three-helix bundle. It contains no cysteines or disulfides that could be reduced and contribute to unfolding in cells. We randomized 13 residues along the first and second helices using NNK codons[2] (**Fig. 1b**) to generate an mRNA-displayed protein library containing $5 \times 10^{13}$ unique Z variants. After 12 rounds of selection, we sequenced the enriched cDNA library and analyzed the binding of 20 candidates with two consensus sequences. Because of their binding properties we selected three Zdk variants for further use (**Fig. 1c**). In a radiometric binding assay Zdk1, the candidate with the greatest difference in affinity for LOV's lit versus dark states, had 26.2 nM affinity for a LOV2 mutant fixed in the dark state (C450A, ref. 3) but $K_d$ > 4 μM for a lit-state mutant (I539E, ref. 4) (**Fig. 1c**). A model based on this affinity showed that caging was optimal when the mitochondrial anchor was expressed at 5–10-fold excess over the other component (**Fig. 1d**). The crystal structure of LOV2 complexed with Zdk1 revealed that LOV2's C-terminal helix Jα, which unwinds upon irradiation[5], was inserted into a pocket formed by the first two helices of Zdk1 (**Fig. 1e**, **Supplementary Figs. 2** and **3**, **Supplementary Table 1**, and **Supplementary Video 1**). Consistent with this crystal structure, mutations near the LOV2 C terminus abolished binding, while mutations on other portions of the Jα helix had no effect (**Supplementary Fig. 3**). Zdk2 and Zdk3 showed smaller differences in lit–dark affinity (**Fig. 1c**), and their binding did not require interaction with the LOV C-terminal helix (**Supplementary Figs. 2** and **4** and **Supplementary Table 1**). Zdk2 and Zdk3 will be useful in applications in which proteins must be appended to the LOV C terminus.

To examine the kinetics of protein activation and inactivation using LOVTRAP in living cells, we fused the N terminus of LOV2 to mCherry fluorescent protein and the N terminus of Zdk to a fragment of TOM20, a mitochondrial anchoring sequence[6]. When we coexpressed the two proteins in HeLa cells, mCherry was localized at mitochondria in the dark but generated diffuse

[1]Department of Pharmacology, University of North Carolina at Chapel Hill, Chapel Hill, North Carolina, USA. [2]Lyda Hill Department of Bioinformatics, UT Southwestern Medical Center, Dallas, Texas, USA. [3]Department of Biomolecular Mechanisms, Max Planck Institute for Medical Research, Heidelberg, Germany. [4]Department of Biochemistry and Biophysics, University of North Carolina at Chapel Hill, Chapel Hill, North Carolina, USA. [5]Eshelman School of Pharmacy, University of North Carolina at Chapel Hill, Chapel Hill, North Carolina, USA. [6]Carolina Center for Genome Sciences, University of North Carolina at Chapel Hill, Chapel Hill, North Carolina, USA. [7]Lineberger Cancer Center, University of North Carolina at Chapel Hill, Chapel Hill, North Carolina, USA. [8]Present address: Institute of Biochemistry, Graz University of Technology, Graz, Austria. [9]These authors contributed equally to this work. Correspondence should be addressed to K.M.H. (khahn@med.unc.edu), G.D. (gaudenz.danuser@utsouthwestern.edu), or R.L. (rliu@email.unc.edu).

RECEIVED 21 NOVEMBER 2015; ACCEPTED 16 JUNE 2016; PUBLISHED ONLINE 18 JULY 2016; DOI:10.1038/NMETH.3926

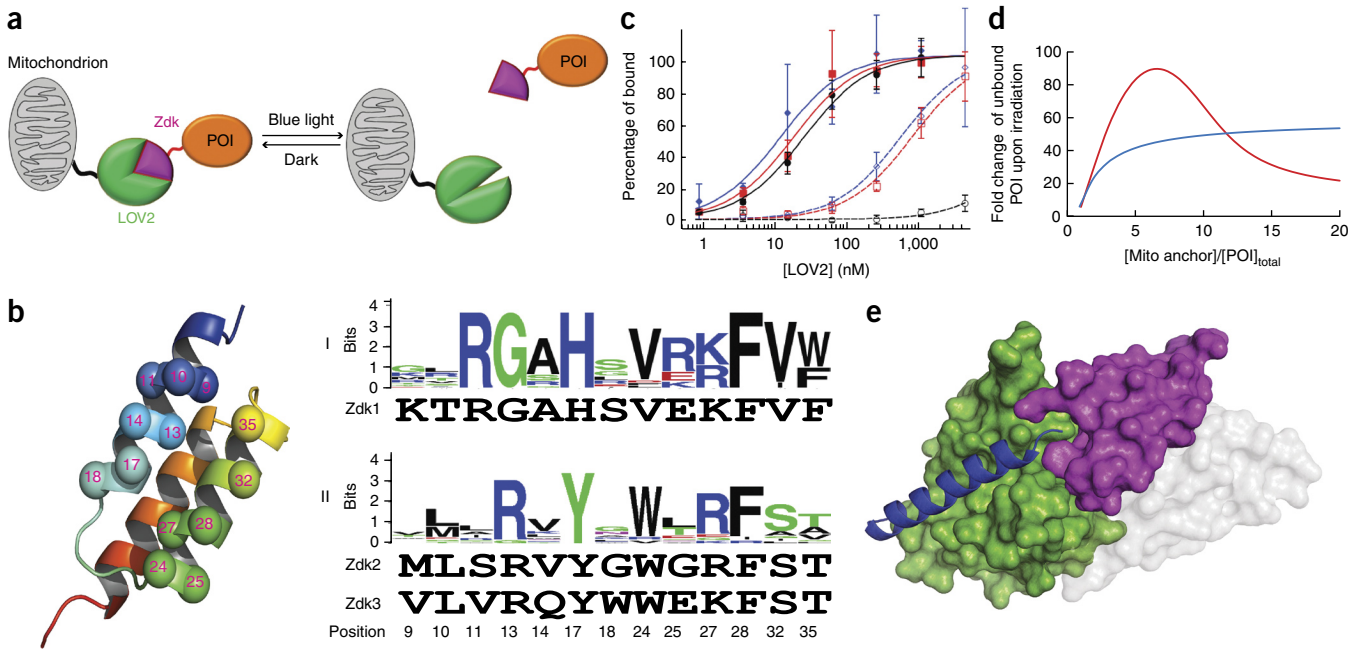


**Figure 1** | Generation of Zdk and design of LOVTRAP. (**a**) Schematic illustration of the LOVTRAP system. POI, protein of interest. (**b**) 13 residues along the first and second helices of the Z domain from protein A were randomized to generate a variable surface (left). Two consensus sequences (indicated here as I and II) bound specifically to the dark state of LOV2 (right). (**c**) Binding of Zdk isoforms to LOV2's dark state (C450A mutant) versus lit state (I539E mutant; $n = 4$ for each curve). Dark versus lit affinities of Zdk1 (black), Zdk2 (red), and Zdk3 (blue) were 26.2 ± 2.2 nM versus >4 μM, 17.0 ± 3.9 nM versus 761 ± 78 nM, and 11.4 ± 3.6 nM versus 537 ± 37 nM, respectively. Error bars are the s.d. of replicates. (**d**) A model showing the amount of protein released upon irradiation depending upon the relative expression levels of the mitochondrial (mito) anchor and the POI for Zdk1 fused to the POI and LOV2 targeted to mitochondria (red) or vice versa (blue). (**e**) Crystal structure of the LOV2–Zdk1 complex. Zdk1 (magenta) docks on the core domain of LOV2 (green) and the C-terminal residues of the LOV2 Jα helix (blue).

cytoplasmic distribution within 1 s after irradiation with 450–490-nm light (**Fig. 2a**, **Supplementary Fig. 4**, and **Supplementary Video 2**). The release or return of mCherry from or to the mitochondria was not impaired by repeated cycling between the lit and dark distributions for at least ten times (**Fig. 2b**). LOV mutants incapable of undergoing light-induced conformational changes did not release proteins from the mitochondria even after prolonged irradiation (**Supplementary Fig. 5** and **Supplementary Video 3**). For wild-type LOV2, the half-life ($t_{1/2}$) for return of diffuse mCherry to the mitochondria was 18.5 s (**Fig. 2c**). These kinetics were tunable through the introduction of known and novel mutations in the LOV2 domain (**Supplementary Table 2**)[7,8], enabling us to vary the $t_{1/2}$ of return from 1.7 to 496 s (**Fig. 2c**). Fast rates are useful to control signaling with precise kinetics, while slow kinetics enable continuous activation with minimal irradiation (e.g., the V416L mutant will maintain greater than 80% activity with a 1-s light pulse every 2.5 min). Finally, we tested the ability of LOVTRAP to reversibly anchor the POI at points other than mitochondria; fusion of Zdk with an N-terminal fragment of Lyn kinase[9] led to reversible translocation of LOV2 between the cytosol and plasma membrane (**Supplementary Fig. 6a** and **Supplementary Video 4**).

Regulatory processes controlling cell-edge protrusion and retraction are driven by feedback interactions among signaling proteins[10,11]. At steady state, the cell edge oscillates on a time scale of 1–5 min[12]. We leveraged the kinetic control of LOVTRAP to mimic the activation and deactivation of signals that drive these oscillations, focusing on the GTPases Rac1

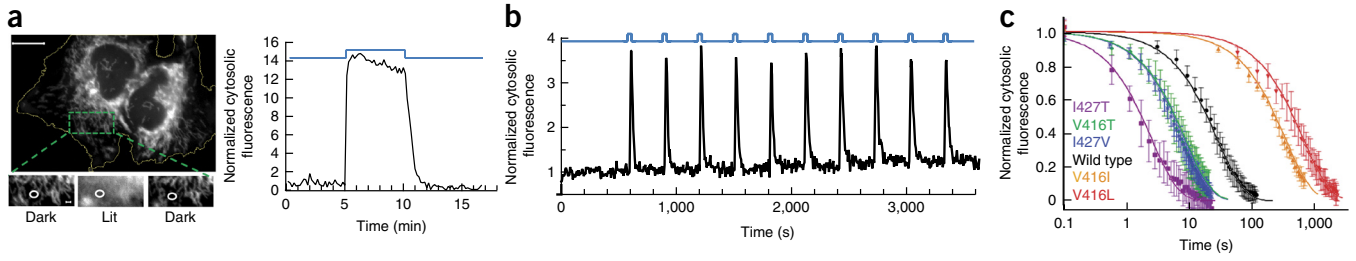


**Figure 2** | Protein control by LOVTRAP. (**a**) HeLa cells expressing mCherry fused to LOV2 and Zdk1 targeted to the outer membrane of mitochondria (left). Fluorescence intensity (right) monitored at a spot devoid of mitochondria (circles in lower images; blue, irradiation). Dashed green box indicates area magnified in the images in the bottom of panel **a**. Scale bars, 10 μm (upper) and 1 μm (lower). (**b**) Repeated irradiation cycles. (**c**) Effects of LOV2 mutants on return $t_{1/2}$ (mean ± s.d. in seconds): I427T (purple, $n = 18$), 1.7 ± 0.6; V416T (green, $n = 12$), 5.0 ± 2.0; I427V (blue, $n = 15$), 5.5 ± 0.8; wild type (black, $n = 12$), 18.5 ± 3.7; V416I (orange, $n = 3$), 239 ± 5; V416L (red, $n = 6$), 496 ± 38.

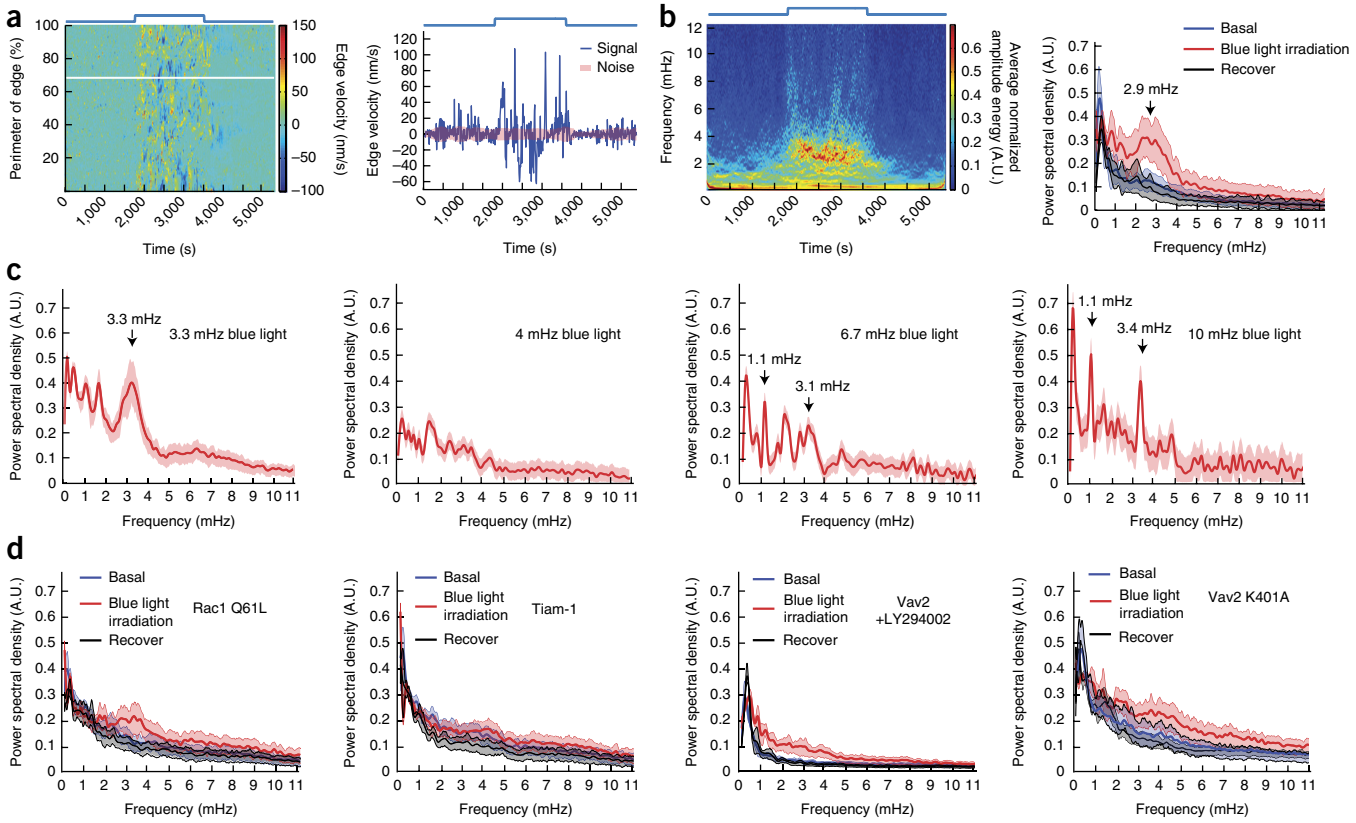


**Figure 3** | Resonance in HeLa cell protrusion–retraction cycles upon acute release of Vav2. (**a**) Kymograph of cell-edge velocity (*y*-axis, distance along cell perimeter; *x*-axis, time; left panel). Time series of instantaneous edge velocity sampled at one cell-edge location (right panel), indicated in the left panel by a white horizontal line. Red area, noise band as determined by empirical mode decomposition of the time series (see Online Methods). Blue lines at the top of each panel show the timing and duration of irradiation. (**b**) Left, representative spectrogram of HeLa-cell-protrusion cycles in response to Vav2 release (blue line indicates irradiation). Right, power density as a function of the temporal frequency of cell-edge protrusion–retraction cycles, separated into before (blue), during (red), and after (gray) release of Vav2. Center line indicates median density, band indicates 95% confidence interval about median, calculated from 2,606 edge locations sampled in 7 cells. A.U. indicates that power spectral densities are expressed in arbitrary units comparable between panels. (**c**) Power densities from cells stimulated with 3.3 mHz, 4 mHz, 6.7 mHz, and 10 mHz blue light pulses. Center line and confidence bands as in **b**. For each panel, 2,044 edge locations sampled in 6 cells. (**d**) Changing power densities during acute stimulation of constitutively active Rac1Q61L (357 edge locations, 2 cells), endogenous Rac1 via release of Tiam1 DH–PH domain (1,546 edge locations, 4 cells), constitutively active Vav2 in the presence of the PI3K inhibitor LY294002 (2,350 edge location, 7 cells), and Vav2 K401A mutant with impaired binding to PI3K-generated phospholipid products (1,439 edge locations, 4 cells).

and RhoA and their upstream GTP exchange factor Vav2. In order to control these proteins' activity without influence from endogenous regulatory pathways, we fused Zdk to constitutively active mutants of RhoA (Q63L) and Rac1 (Q61L) and to a constitutively active fragment of Vav2 (amino acids 185–575, ref. 13, **Supplementary Table 3**). In HeLa cells, release of each protein (henceforth referred to as protein 'activation') produced different specific effects on edge velocity, ruffling, cell area, and protrusion distribution (**Supplementary Figs. 6–8** and **Supplementary Videos 5–7**). Before irradiation, expression of LOVTRAP Vav2, LOVTRAP Rac1, and LOVTRAP RhoA had little effect on endogenous Rac1 expression, cell-edge protrusion, or mitochondrial function (**Supplementary Figs. 9–12**).

To further analyze the protrusion and retraction events induced by activation of Vav2, Rac1, and RhoA, we tracked the cell edge before, during, and after optogenetic stimulation (**Supplementary Video 8**) and quantified the behavior in an edge-velocity kymograph, where each row represents the velocity evolution of a particular location on the cell edge over time (**Fig. 3a**)[12]. Strikingly, activation of Vav2 did not just induce a spike of positive velocity; instead, it generated a sustained increase in protrusion and retraction velocities. This suggested that Vav2 signaling contributes to both protrusion and retraction responses.

We suspected that frequency spectra of protrusion–retraction cycles would undergo changes during Vav2 activation and deactivation, as elevated Vav2 activity would gradually turn on different downstream effector pathways with different response kinetics. We therefore implemented the Hilbert–Huang transform[14] to define for each location along the cell edge an instantaneous frequency density spectrum (see Online Methods and **Supplementary Fig. 13**). We integrated spectra from all locations into a per-cell spectrogram (**Fig. 3b**, left) and temporally averaged the periods before, during, and after Vav2 activation (**Fig. 3b**, right). Before and after activation the spectra displayed a unimodal distribution with a peak at ~0.5 mHz, corresponding approximately to the inverse of the 1,800-s time window of observation. Upon Vav2 activation, a peak emerged at 2.9 mHz, reflecting a global stimulation of protrusion–retraction cycles of ~330 s. Owing to the regularity of this response across a cell population,

we hypothesized that ~3 mHz reflected the principal frequency of a resonator. To test this we exploited the kinetic control and rapid reversibility of LOVTRAP–Vav2 to optogenetically entrain oscillatory cycles. Indeed, pulses of blue light of 50 s 'on' and 250 s 'off' generated highly synchronized protrusion–retraction cycles with a 3.3-mHz frequency (**Fig. 3c** and **Supplementary Fig. 14a**). Cycles could not be entrained when exposing LOVTRAP–Vav2 to pulses of 50 s on and 200 s off (4 mHz), whereas pulses of 6.7 mHz and 10.0 mHz—i.e., multiples of the putative principal resonator frequency—did entrain cycles, but again at 3.3 mHz (**Fig. 3c** and **Supplementary Fig. 14b**), further supporting the resonator hypothesis. In all experiments we observed several peaks at frequencies below 3.3 mHz. These may be the product of secondary resonating circuits, or they may represent lower harmonics of the primary resonator, such as the peaks at 1.1 mHz.

Our data suggested that Vav2 is part of an activator circuitry that stimulates protrusion, most probably through its role as an activating guanine nucleotide exchange factor (GEF) of Rac1 GTPase, which drives actin-filament assembly and lamellipodium formation[15] (**Supplementary Fig. 15**). To test this we used a LOVTRAP construct to acutely release Rac1Q61L and performed spectral analysis (**Fig. 3d** and **Supplementary Fig. 14c**). Compared to the Vav2 response, the Rac1-induced oscillations showed a mild frequency density increase between 3 and 4 mHz. The absence of a resonator response could be related to the fact that Rac must be modulated by GTPase regulatory pathways to restore the circuitry. Therefore, we repeated these experiments by producing a LOVTRAP construct for the Rac1-specific-GEF Tiam1. Acute release of Tiam1 also had no effect on the spectra (**Fig. 3d** and **Supplementary Fig. 14c**). Hence, activation of cells with Vav2 promotes both the stimulation and the restoration required for cyclic protrusion and retraction.

Vav2 interacts with phospholipid products of the phosphoinositide 3-kinase (PI3K)[16]. These are thought to localize at the protruding cell edge via association of PI3K with focal adhesions[17] and/or via direct or indirect activation of PI3K downstream of Rho-family GTPases[15,18]. We tested whether inhibition of PI3K would abolish the protrusion–retraction resonator. We found no resonance when we irradiated cells expressing LOVTRAP–Vav2 if the medium contained the PI3K inhibitor LY294002 (**Fig. 3d** and **Supplementary Fig. 14c**). Furthermore, a LOVTRAP–Vav2 construct harboring a point mutation of Vav2's pleckstrin homology (PH) domain that lowers interaction with lipid products[19] did not result in a pronounced narrowband resonance, even though optogenetic release of this construct stimulated protrusion–retraction cycles over a broad range of frequencies (**Fig. 3d** and **Supplementary Fig. 14c**).

LOVTRAP uses the Zdk reagents in a simple and versatile approach that can be applied to many proteins. Protein release occurs with subsecond kinetics and reversibility can be tuned from <3 to ~500 s. The Zdk reagents can be used as building blocks for other optogenetic tools, providing light-induced dissociation with >150-fold change in affinity. We demonstrate LOVTRAP's precise and reversible control of activation kinetics by exploring a signaling circuit that governs cell-edge oscillations, revealing a natural resonance frequency and an essential role for Vav2. We anticipate that, in a similar manner, LOVTRAP can shed light on the host of processes that rely on oscillating cellular signals.

## METHODS

Methods and any associated references are available in the online version of the paper.

**Accession codes.** Atomic coordinates and structure factors have been deposited in the Protein Data Bank under accession codes 5EFW (LOV2–Zdk1 complex), 5DJT (LOV2–Zdk2 complex), and 5DJU (LOV2–Zdk3 complex); and in GenBank under accession codes KX429612 (Zdk1), KX429613 (Zdk2), and KX429614 (Zdk3).

*Note: Any Supplementary Information and Source Data files are available in the online version of the paper.*

### ACKNOWLEDGMENTS

This work was funded by NIH grants R01-GM090317 (K.M.H. and G.D.), P01-GM103723 (K.M.H. and G.D.), R01-DA036877 (K.M.H. and B.K.), and R01-CA157738 (R.L.) and by the Max Planck Society, German Research Foundation DFG, FOR 1279 (I.S.). H.W. is a recipient of an Arthritis Foundation Postdoctoral Fellowship. We thank E. Hartmann for crystallizing Zdk–LOV complexes, R. Littlefield (UNC Chapel Hill Department of Biochemistry and Biophysics) for providing LOV2 peptides, and E. Trudeau for cloning help. Diffraction data were collected at the Swiss Light Source, beamline X10SA, of the Paul Scherrer Institute, Villigen, Switzerland. We thank the Heidelberg data collection team and the PXII staff for their support in setting up the beamline and C. Roome for expert support of the crystallographic software. The UNC Flow Cytometry Core Facility is supported in part by P30 CA016086 Cancer Center Core Support Grant to the UNC Lineberger Comprehensive Cancer Center.

### AUTHOR CONTRIBUTIONS

H.W. performed the screening experiments, engineered proteins, and performed imaging studies. M.V. performed analysis of oscillating signaling behavior. A.W., M.T., and I.S. carried out crystallography. H.W., H.Y., and B.K. purified proteins for crystallography. R.L., G.D., and K.M.H. directed the work and carried out final edits for the paper, which was written using contributions from all authors.

### COMPETING FINANCIAL INTERESTS

The authors declare no competing financial interests.



1. Weitzman, M. & Hahn, K.M. *Curr. Opin. Cell Biol.* **30**, 112–120 (2014).
2. Nord, K. *et al. Nat. Biotechnol.* **15**, 772–777 (1997).
3. Kay, C.W. *et al. J. Biol. Chem.* **278**, 10973–10982 (2003).
4. Harper, S.M., Christie, J.M. & Gardner, K.H. *Biochemistry* **43**, 16184–16192 (2004).
5. Harper, S.M., Neil, L.C. & Gardner, K.H. *Science* **301**, 1541–1544 (2003).
6. Kanaji, S. *et al. J. Cell Biol.* **151**, 277–288 (2000).
7. Zoltowski, B.D., Vaccaro, B. & Crane, B.R. *Nat. Chem. Biol.* **5**, 827–834 (2009).
8. Kawano, F. *et al. PLoS ONE* **8**, e82693 (2013).
9. Levskaya, A. *et al. Nature* **461**, 997–1001 (2009).
10. Krause, M. & Gautreau, A. *Nat. Rev. Mol. Cell Biol.* **15**, 577–590 (2014).
11. Vicente-Manzanares, M., Webb, D.J. & Horwitz, A.R. *J. Cell Sci.* **118**, 4917–4919 (2005).
12. Machacek, M. & Danuser, G. *Biophys. J.* **90**, 1439–1452 (2006).
13. Abe, K. *et al. J. Biol. Chem.* **275**, 10141–10149 (2000).
14. Huang, N.E. & Shen, S.S. (eds.) *Hilbert-Huang Transform and Its Applications* 2nd edn. (World Scientific, 2014).
15. Yang, H.W. *et al. Mol. Cell* **47**, 281–290 (2012).
16. Han, J. *et al. Science* **279**, 558–560 (1998).
17. Chen, H.C. & Guan, J.L. *Proc. Natl. Acad. Sci. USA* **91**, 10148–10152 (1994).
18. Weiner, O.D. *et al. Nat. Cell Biol.* **4**, 509–513 (2002).
19. Booden, M.A., Campbell, S.L. & Der, C.J. *Mol. Cell. Biol.* **22**, 2487–2497 (2002).

## ONLINE METHODS

**Z-library construction.** The synthetic gene encoding the Z library was assembled by annealing and enzymatically extending primers ZL-U141 and ZL-B143 (**Supplementary Table 4**, Genelink, NY) that have complementary 3′ ends. Codon NNK (N = G, A, C, T; K = G, T) was used to encode randomized residues. The resulting dsDNA was amplified by PCR using primers ZL-5-66 and ZL-3-57 (**Supplementary Table 4**). The cycle numbers were optimized to avoid overamplification by running small-scale PCR reactions and checking the product from different cycles on 2% agarose gels. A small portion of the final cDNA library was cloned into pJet1.2 vector (Thermo Scientific) and transformed into NEB5α-competent cells. 95 colonies were picked and sequenced to check the codon bias.

**mRNA display.** The C450A and I539E mutants of the LOV2 domain of *Avena sativa* (oat) phototropin1 (404–546) were cloned into the bacterial expression vector pProEx–HTb containing N-terminal $His_6$ tag followed by an Avi tag. The proteins were expressed in *Escherichia coli* strain CVB101 (Avidity). They were induced using 0.5 mM isopropyl β-D-1-thiogalactopyranoside (IPTG, Sigma) with 100 μM biotin (Sigma) to express biotinylated LOV2 proteins, or they were induced with 0.5 mM IPTG without biotin to express unbiotinylated LOV2 proteins. The proteins were purified using a HisTrap FF column (GE Healthcare).

The mRNA–protein fusion library was generated and purified according to our published protocol[20]. Reverse transcription was performed to convert the mRNA–protein into cDNA/mRNA–protein form. The purified fusion library was diluted in a binding buffer (50 mM Tris-HCl pH 7.5, 150 mM NaCl, 0.05% Tween-20, 1 mg/mL BSA, 1 mg/mL yeast tRNA, and 0.5 mM EDTA) and passed through 75 μL Streptavidin UltraLink Plus Resin (Thermo Scientific) pretreated with 1 mg/mL BSA and 1 mg/mL yeast tRNA to minimize the sequences that nonspecifically bound to streptavidin and/or the matrix. The flowthrough was incubated with LOV2 C450A preimmobilized on 75 μL streptavidin beads for 90 min at room temperature. In rounds 1–5, the beads were washed with 300 μL washing buffer (50 mM Tris-HCl pH 7.5, 150 mM NaCl, 0.05% Tween-20), while in rounds 6–12, the beads were washed with 300 μL washing buffer containing 5 mg/mL LOV2 I539E to minimize the enrichment of sequences that bound to the lit form of LOV2, followed by a wash with 300 μL washing buffer. In rounds 1–5, the selected library was eluted by incubating the beads with 150 μL eluting buffer (50 mM Tris-HCl pH 7.5, 150 mM NaCl, 0.05% Tween-20, 1.5 mM $MgCl_2$) containing 1 U RNase H (Thermo Scientific) for 120 min at 37 °C, while in rounds 6–12 the selected library was competitively eluted by incubating the beads with 300 μL eluting buffer containing 5 mg/mL LOV2 C450A for 60 min at room temperature. The elution was treated with 1 U protease K for 60 min at room temperature, followed by phenol–chloroform extraction to remove protein components. The enriched cDNA library was regenerated by PCR using primers ZL-5-66 and ZL-3-57.

After 12 rounds of selection, the enriched DNA library was cloned into the pJet1.2 vector and transformed into DH5α. 120 colonies were picked for sequencing.

**Radiometric binding assay.** The sequences from the selected library were translated *in vitro* in the presence of $^{35}S$-methionine, followed by purification using HisPur Cobalt Resin (Thermo Scientific). The purified proteins were incubated with different concentrations of biotinylated LOV2 mutants in 96-well filter plates (Pall) at room temperature for 30 min. 20 μL Streptavidin UltraLink Plus Resin was added, and the suspension was shaken for 60 min. The flowthrough was removed, and the beads were washed with three bed volumes of washing buffer. 200 μL scintillation liquid was added in each well, and the top of the plate was sealed using a transparent sealer. The plate was rotated to mix well, then read using a scintillation plate reader.

**Bio-layer interferometry (BLI) assay.** GST–Zdk1 protein and LOV2 wild type were expressed and purified as described above. The binding kinetics were determined using an Octet QKe system (forteBio). Anti-GST biosensors were equilibrated in an assay buffer (phosphate-buffered saline with 1 mg/ml BSA and 0.05% Tween-20) for 60 s, then the tips were loaded with 100 nM GST–Zdk1 for 300 s. The association and dissociation of LOV2 proteins were examined by incubating the Zdk-loaded tips with 50, 100, 200, and 500 nM LOV2 proteins for 300 s and then in assay buffer for 300 s. Kinetics data were analyzed using forteBio software (forteBio). The curves were fit globally using a 1:1 model.

**Protein crystallization.** The C450A mutant of the LOV2 domain of *Avena sativa* (oat) phototropin1 (404–546) was cloned into the bacterial expression vector pGEX (GE Healthcare) containing an N-terminal GST-tag and $His_6$-tag followed by a TEV protease cleavage site. The Zdk1, Zdk2 and Zdk3 proteins were cloned into pQE-80L (Qiagen) containing an N-terminal $His_6$-tag followed by a TEV protease cleavage site. The proteins were purified using a HisTrap FF column (GE Healthcare).

After elution from the HisTrap FF column using a linear gradient of 10–500 mM imidazole in the same buffer, the proteins were mixed with TEV protease using a 1:20 molar ratio of TEV:substrate and dialyzed overnight at 4 °C against TEV buffer (50 mM Tris-HCl pH 7.5, 100 mM NaCl, 1 mM dithiotreitol). The dialyzed sample was loaded onto the HisTrap FF column to remove cleaved $His_6$–TEV. The flowthrough was concentrated and subjected to gel-filtration chromatography on a Superdex 75 column (GE Healthcare) equilibrated with TEV buffer. The eluted protein was concentrated, aliquoted, frozen in liquid nitrogen, and stored at −80 °C.

Crystallization was performed at 20 °C in the dark using the vapor-diffusion method. Crystal handling was done under orange light with a 2 mm thick OG570 filter (Schott, Germany) shielding the microscope bulb. To allow complex formation of LOV2(C450A) and Zdk1, both proteins were incubated for 60 min in a 1:1 molar ratio in washing buffer. The complexes of LOV2(C450A) with Zdk2 or Zdk3 were formed by mixing both components in a 1:1 stoichiometry and incubating for 30 min on ice. Crystals of LOV2–Zdk1 were obtained by mixing equal volumes of protein solution (at 10.0 mg/ml) with 2 M $(NH_4)_2SO_4$, 0.1 M sodium citrate pH 3.5 reservoir solution. Tetragonal crystals of the LOV2–Zdk1 complex grew to final dimensions within 1 week. For cryoprotection, crystals were transferred to reservoir solution containing 25% (v/v) glycerol and, after 1 min incubation, crystals were cryocooled in liquid nitrogen. Box-shaped crystals of LOV2–Zdk2 complex were grown by mixing equal volumes of

preformed protein complex solution (at 15.7 mg/ml), reservoir solution containing 0.1 M trisodium citrate pH 5.6, 0.2 M ammonium acetate, 32% (w/v) PEG 4000, and 0.1 M copper(II) chloride solution as an additive. Before flash-cooling in liquid nitrogen the crystals were briefly washed in cryoprotectant solution consisting of the reservoir solution with PEG 4000 concentration increased to 40% (w/v). Rod-shaped crystals of LOV2–Zdk3 complex were obtained by mixing equal volumes of preformed protein complex solution (at 16.5 mg/ml) and reservoir solution containing 0.1 M citric acid pH 4.0, 1.0 M lithium chloride, and 18% (w/v) PEG 6000. Crystals were briefly rinsed in cryoprotectant solution composed of the corresponding reservoir solution supplemented with 20% (v/v) glycerol before flash-cooling in liquid nitrogen.

**X-ray diffraction data collection and structure determination.** Single crystal X-ray diffraction data were collected at 100 K on the X10SA beamline at the Swiss Light Source (Paul Scherrer Institute, Villigen, Switzerland). The data were processed with XDS[21]. All three structures of LOV2–Zdk complexes were determined by molecular replacement using Phaser[22]. The structure of LOV2–Zdk1 was determined with individual search models of LOV2 (PDB entry 2V0U) and protein Z (PDB entry 1LP1, chain A). A unique solution was obtained for one molecule each in the asymmetric unit. However, initial density maps suggested the presence of another protein Zdk1 molecule with altered N-terminal helix conformation that was manually added during the initial rounds of refinement. The structure of the LOV2–Zdk2 complex was determined using LOV2 domain coordinates from PDB entry 2WKQ and a homology model of Zdk2 (residues 9–58) generated with SWISS-MODEL[23] based on PDB entry 2KZJ as a search model. The structure of the LOV2–Zdk3 complex was determined using the same LOV2 coordinates and a homology model of Zdk3 (residues 9–58) based on PDB entry 1Q2N. The final models were optimized in iterative cycles of manual rebuilding using Coot[24] and refinement using phenix.refine[25]. Data collection and refinement statistics are summarized in **Supplementary Table 5**. Model quality was validated using validation methods implemented in PHENIX[26].

**Plasmid construction and transfection.** All plasmids were generated by overlap PCR and subcloned into mammalian expression vector pTriEx by restriction enzyme digestion and ligation. The plasmids (**Supplementary Table 6**) were cotransfected into the cells using FuGene 6 (Promega), following the manufacturer's instructions.

**Cell lines.** All cell lines were obtained from the American Type Culture Collection (ATCC, Manassas, Virginia) and were tested for mycoplasma by the UNC Tissue Culture Core Facility. No cells on the ICLAC list of commonly misidentified cells were used in this work.

**Western blotting.** HeLa cells were transiently cotransfected with LOVTRAP plasmids for 20 h before lysis in RIPA buffer. The cell extracts were adjusted to the same amount of total cellular protein (50 µg) and electrophoresed in a 4–15% gradient polyacrylamide gel. After electrophoretic transfer to a PVDF membrane at 1.0 A for 30 min, the membranes were blocked with TBST buffer (50 mM Tris-HCl, pH7.5, 150 mM NaCl, 0.05% Tween-20) containing 5% BSA for 1 h at room temperature. The primary antibodies (mouse monoclonal anti-Rac1 antibody from Cytoskeleton, Inc., Cat# ARC03, 1:500 dilution[27]; mouse monoclonal anti-GFP Antibody from Clontech, Cat# 632381, 1:1,000 dilution[28]; and mouse monoclonal anti-human vinculin antibody Clone h-VIN1 from Sigma, Cat# V9131, 1:200 dilution[29]) in TBST were placed on the membrane and incubated at 4 °C overnight. After three washings with TBST over 5 min, the second antibody (anti-mouse IGG conjugated with DyLight680, from Cell Signaling, Cat#5470P, 1:10,000 dilution[30]) was applied. After three washings with TBST over 5 min, the membrane was scanned by the Odyssey Infrared Imaging System (LI-COR Biosciences, Lincoln, NE).

**Flow cytometry.** HeLa cells were transiently cotransfected with LOVTRAP plasmids for 20 h, then rinsed, trypsinized, washed, and resuspended in fresh DPBS buffer at a density of 106 cells/ml. 5 µM DilC1(5) or MitoSOX Red were added to the cells, and the cells were then incubated at 37 °C for 30 min according to Mukhopadhyay *et al.*[31]. Samples were analyzed using an LSR II flow cytometer (BD Biosciences) at the UNC Flow Cytometry Core Facility. The gate was set so that only cells labeled with dyes were displayed.

**Live cell imaging.** HeLa cells were transiently cotransfected with LOVTRAP plasmids 20–28 h before imaging. Cells used for live cell imaging were seeded on coverslips coated with 10 mg/ml fibronectin in Ham's F-12K medium free of Phenol Red and containing 0.5% fetal bovine serum (FBS). Coverslips were mounted in an Attofluor live cell chamber (Invitrogen) and placed on a heated microscope stage (Warner). Images were acquired using an Olympus IX81-ZDC microscope equipped with a CoolSNAP HQ2 14-bit camera (Photometrics). Bandpass and neutral density filters (Chroma) were switched using motorized filter wheels (Ludl Electronic Products) controlled by Metamorph Software version 7.6.4. YFP and mCherry images were acquired using a 100 W Hg arc lamp with a 1% ND filter and a 510–520 nm or 565–595 nm band-pass filter respectively, for 500 ms. For photoactivation, a 5% ND filter and a 426-446 nm band-pass filter were used. Unless otherwise indicated, activation was carried out using a pulse protocol alternating 5 s light with 5 s dark. This minimizes photodamage while maintaining greater than 80% activity for wild-type LOV2. Images were processed postacquisition via shading correction, background subtraction, and binary masking using Metamorph software (Molecular Devices).

**Blind scoring.** Images from VAV2 or RhoA activation were mixed with images from control cells, and a naïve observer was asked to score the cells, stating whether the blue light induced or reduced ruffling.

**Image analysis.** Cell outlines were identified using intensity based thresholding on all frames of time lapse movies (**Supplementary Video 8**). The cell edge was subsequently divided into 1µm segments, or windows, where the average normal velocity vector was calculated by tracking these segments from one frame to the next. A velocity profile for each window was built using the signed normal vector magnitude of the respective window. The cell-edge velocity map (as shown in the main text, **Fig. 3a**) was constructed




doi:10.1038/nmeth.3926

by stacking up the velocity profiles from all windows, as described in Vilela *et al.*, 2013 (ref. 32).

**Edge velocity frequency analysis.** A signal processing technique known as Hilbert–Huang transform was used to analyze the time-frequency content of the edge velocity profiles over time[14]. In a first step this technique applies the empirical mode decomposition algorithm (EMD) to decompose the signal into monochromatic components (components with only one frequency at each time point). **Supplementary Figure 13** shows an example, in which a test signal is decomposed into eight empirical modes. Subsequently, each mode is Hilbert transformed and used to build a mathematical construct referred to as a Hilbert spectrum. Two important features were inferred from the spectrum at all time points of a time series: the instantaneous frequency spectrum defined by the combination of frequencies of the monochromatic modes and their respective amplitudes. The final time series spectrum was obtained by arranging instantaneous frequencies and amplitudes over time for all decomposed components, as shown in the **Supplementary Figure 13** box.

Each signal extracted from a window of a given cell gave rise to one time-frequency spectrum. The spectrum for a given cell was then obtained by bootstrapping the mean amplitude for each time-frequency pair of all windows[33] (**Supplementary Fig. 13** flowchart). The same bootstrapping procedure was applied to obtain a final spectrum extracted from several cells. To allow combination of cells with different ranges of protrusion–retraction velocity each individual cell spectrum was first normalized. A specific bootstrap technique for frequency domain data was used to avoid bias from dominant cells or cell windows[14].

**Code availability.** Software code for spectral analysis of protrusion behavior is available as **Supplementary Software**.


20. Cotton, S.W., Zou, J., Valencia, C.A. & Liu, R. *Nat. Protoc.* **6**, 1163–1182 (2011).
21. Kabsch, W. *Acta Crystallogr. D Biol. Crystallogr.* **66**, 125–132 (2010).
22. McCoy, A.J. *et al. J. Appl. Cryst.* **40**, 658–674 (2007).
23. Arnold, K. *et al. Bioinformatics* **22**, 195–201 (2006).
24. Emsley, P. *et al. Acta Crystallogr. D Biol. Crystallogr.* **66**, 486–501 (2010).
25. Afonine, P.V. *et al. Acta Crystallogr. D Biol. Crystallogr.* **68**, 352–367 (2012).
26. Adams, P.D. *et al. Acta Crystallogr. D Biol. Crystallogr.* **66**, 213–221 (2010).
27. Seidelin, J.B. *et al. Am. J. Physiol. Gastrointest. Liver Physiol.* **308**, G92–G99 (2015).
28. Lorenz, H., Hailey, D.W. & Lippincott-Schwartz, J. *Nat. Methods* **3**, 205–210 (2006).
29. Risse, P.A. *et al. Am. J. Physiol. Lung Cell. Mol. Physiol.* **300**, L958–L966 (2011).
30. Jia, L. *et al. Mol. Biol. Cell* **22**, 4227–4235 (2011).
31. Mukhopadhyay, P. *et al. Nat. Protoc.* **2**, 2295–2301 (2007).
32. Vilela, M. *et al. Methods Enzymol.* **519**, 253–276 (2013).
33. Zoubir, A.M. & Iskander, D.R. *Bootstrap Techniques for Signal Processing* (Cambridge University Press, 2004).